The Accuracies of Crossover and Parallel-Track Estimates of Geostrophic Velocity from TOPEX/Poseidon and Jason Altimeter Data

MICHAEL G. SCHLAX AND DUDLEY B. CHELTON

College of Oceanic and Atmospheric Sciences, Oregon State University, Corvallis, Oregon

(Manuscript received 23 August 2002, in final form 4 February 2003)

ABSTRACT

Mean-squared errors of surface geostrophic velocity estimates from the crossover and parallel-track methods are calculated for altimeters in the Ocean Topography Experiment (TOPEX)/Poseidon and Jason orbits. As part of the crossover method analysis, the filtering properties and errors of cross-track speed estimates are examined. Velocity estimates from both the crossover and parallel-track methods have substantial mean-squared errors that exceed 20% of the signal standard deviation, differ systematically between the zonal and meridional components, and vary with latitude. The measurement errors on the zonal and meridional velocity component estimates from both methods increase at low latitudes owing to the inverse dependence of geostrophic velocity on the Coriolis parameter. Additional latitudinal variations result for the parallel-track method because of the poleward convergence of the satellite ground tracks and the presence of orbit error, and for the crossover method because of the changing angle between the ascending and descending ground tracks. At high latitudes, parallel-track estimates, have elevated measurement errors in both components, while only the zonal component is so affected for the crossover method. Along-track smoothing is efficient for mitigating measurement errors for crossover estimates, and the filtering properties of the smoothed estimates are simply related to the spectrum of cross-track speeds. Such smoothing is less effective for parallel-track estimates, and the filtering properties are more difficult to characterize because of the sampling geometry and the convergence of the parallel ground tracks at high latitudes.

If suitable along-track smoothing is applied in the crossover method, root-mean-squared errors (rmse's) of about 30% or less of the signal standard deviation can be obtained for each orthogonal velocity component over the latitude range 5°–60°. With 2-cm orbit errors, the parallel-track method yields estimates of the meridional velocity component with errors that exceed 40% at all latitudes. If orbit errors can be reduced to 1-cm standard deviation, the parallel-track method yields an rmse smaller than 30% in both orthogonal components for the latitude range 5°–55°.

1. Introduction

Estimation of the zonal and meridional components of the surface geostrophic velocity field is an important application of satellite altimeter data. The crossover method (Parke et al. 1987; Morrow et al. 1992, 1994) utilizes sea surface height (SSH) data obtained from a satellite placed in an exact-repeat orbit to estimate geostrophic velocity at the intersections of ascending and descending ground tracks. Besides the coarse distribution of the crossover points, another concern with application of the crossover method is the time separation between ascending and descending ground track samples of the crossover location. The temporal variability of the velocity field introduces errors in velocity estimates obtained from the nonsimultaneous crossovers. The requirement that the zonal and meridional components be obtained from a geometrical transformation of nonorthogonal estimates of cross-track speeds introduces further errors that vary with latitude.

In anticipation of a tandem Ocean Topography Experiment (TOPEX)/Poseidon (T/P) and Jason altimeter mission with coordinated orbits, Stammer and Dieterich (1999) devised an alternative to the crossover method that utilizes SSH data obtained from closely spaced, parallel ground tracks sampled simultaneously. The parallel-track method estimates the orthogonal components of geostrophic velocity from between-track differences of SSH. The parallel-track method requires data from a coordinated tandem altimeter mission, while the crossover method may be applied to single or multiple (not necessarily coordinated) altimeter missions.

From simulations based on the characteristics of T/P measurement errors, Leeuwenburgh and Stammer (2002) suggest that the optimal tandem T/P–Jason mission for geostrophic velocity estimation is one for which the ground tracks are offset by a longitudinal shift of about $\delta\phi = 0.75°$ of longitude. A closer track spacing

Corresponding author address: Dr. Dudley B. Chelton, College of Oceanic and Atmospheric Sciences, Oregon State University, 104 Oceanic Administration Bldg., Corvallis, OR 97331-5503.
E-mail: chelton@coas.oregonstate.edu

amplifies the effects of measurement errors (especially orbit errors) while a wider track spacing increases sampling errors from unresolved mesoscale variability. The poleward convergence of the ground tracks results in latitudinally varying filtering properties and error variances for the geostrophic velocity estimates.

Leeuwenburgh and Stammer (2002) compared the crossover and parallel-track methods through a simulation study. The SSH output by a high-resolution, eddy-resolving model of the North Atlantic Ocean circulation (Smith et al. 2000) provided the ''data'' input to the geostrophic velocity estimation schemes. Altimeter data were simulated by sampling the model SSH fields along the satellite ground tracks with various random instrumental and long-wavelength measurement and orbit errors added. The accuracies of geostrophic velocity estimates were assessed by direct comparisons with the model output.

The goal of this paper is to complement the work of Leeuwenburgh and Stammer (2002) by presenting sampling, measurement, and total errors for estimates of the zonal and meridional components of geostrophic velocity from the crossover and parallel-track methods applied to SSH data from T/P and Jason. Geostrophic velocity fields can also be computed from smoothed and gridded SSH fields (e.g., Qiu 1995; Ducet et al. 2000; Ducet and Le Traon 2001). One such ''optimal'' technique was assessed by Leeuwenburgh and Stammer (2002). These methods are not addressed in this paper.

The tandem T/P–Jason mission began on 16 September 2002, when T/P was maneuvered into an interleaved orbit in which neighboring parallel ground tracks separated by 1.42° of longitude are sampled essentially simultaneously by T/P and Jason (a 7-min separation). The results presented here include the errors of parallel-track estimates of geostrophic velocity from this configuration and can also provide guidance for the selection of orbits for future tandem missions.

For the calculations presented here, we assume a covariance model for velocity that is isotropic, is related to SSH by geostrophy, and has a latitudinally varying decorrelation length scale. While certainly an oversimplified description of real oceanic variability, this assumption allows a comparison of the two methods, highlighting their various strengths and weaknesses. As part of the crossover method analysis, a description of the filtering and variance properties of cross-track speed estimates is presented. Parke et al. (1987) and Morrow et al. (1994) have previously examined the measurement error component of the mean-squared error (mse) for the crossover method in terms of the errors in the cross-track speed estimates. Their work is extended here to express the measurement error variances of the zonal and meridional components directly in terms of the SSH measurement errors. The results presented here for the sampling error component of the mean-squared errors of crossover estimates are new.

2. Results

SSH measurements $\tilde{h}$ at equally spaced points along the ground track of a satellite placed in an exact-repeat orbit can be decomposed as

$$\tilde{h}(x_j, t) = \tilde{h}(j\Delta_x, t) = \tilde{h}_j(t) = h_j(t) + \epsilon_j(t) + o_j(t). \quad (1)$$

The along-track index of the measurements is j, the spacing of the measurements along track is Δ_x (6.2 km for T/P), and t is the time of the measurement. The true value h of the SSH is contaminated by random instrumental measurement errors ϵ and long-wavelength orbit and environmental measurement errors o.

The instrumental measurement errors are assumed to be uncorrelated with zero mean and variance σ_ϵ^2, and to be independent of the long-wavelength measurement errors. The value of σ_ϵ is about 2 cm for TOPEX and 3 cm for the *European Remote Sensing Satellite* (*ERS*) altimeters (Chelton et al. 2001). Preliminary analysis indicates that measurement errors from Jason are about 2 cm. Measurement errors of both 2 and 3 cm are considered in the analysis presented here. The long-wavelength errors are assumed to be essentially constant along each track over distances of order 1000 km. It is further assumed that the long-wavelength errors have zero mean and variance σ_o^2 and are uncorrelated between different tracks and repeats. This latter assumption is pertinent only to the parallel-track method; the along-track slope estimation required by the crossover method effectively eliminates all long-wavelength error (cf. section 2a). For a time separation of less than a few days between neighboring ground tracks, errors in the long-wavelength environmental corrections will be highly correlated between two parallel tracks. Most of the environmental measurement error is thus eliminated when differencing SSH between the two tracks (as required by the parallel-track method). The residual environmental measurement error in SSH differences between two parallel tracks is probably less than 1 cm. For the parallel-track method, long-wavelength measurement error can therefore be assumed to be dominated by the orbit error, which is random from track to track with an rms of 2–3 cm for T/P (Chelton et al. 2001).

The SSH is assumed to be a realization of an isotropic, homogeneous, and stationary random process with zero mean, variance σ_h^2, and covariance between locations (x, y, t) and (x_i, y_i, t_i) given by

$$C^{hh}(\mathbf{x} + \mathbf{r}, t + \tau) = \sigma_h^2 \exp\left(-\frac{\|\mathbf{r}\|^2}{s_s^2} - \frac{\tau^2}{s_t^2}\right), \quad (2)$$

where $\mathbf{x} = (x, y)$, $\mathbf{r} = (x - x_i, y - y_i)$, $\tau = t - t_i$, and s_s and s_t are the decorrelation scales in space and time, respectively. Assuming geostrophy, there is an associated vector field of surface currents, $\mathbf{v}$, with zonal and meridional components u and v. Following Bretherton

et al. (1976), the covariances between the geostrophic velocity components and the SSH are

$$C^{uh}(\mathbf{x} + \mathbf{r}, t + \tau) = 2\frac{g}{f}\frac{(y - y_i)}{s_s^2}C^{hh}(\mathbf{x} + \mathbf{r}, t + \tau) \quad \text{and} \qquad (3)$$

$$C^{vh}(\mathbf{x} + \mathbf{r}, t + \tau) = -2\frac{g}{f}\frac{(x - x_i)}{s_s^2}C^{hh}(x + \mathbf{r}, t + \tau), \qquad (4)$$

where g is the gravitational acceleration and f is the Coriolis parameter. Since the SSH field is assumed to be isotropic, the variances of the velocity components are equal and can be shown to be

$$\sigma_u^2 = \sigma_v^2 = 2\frac{g^2}{f^2}\frac{\sigma_h^2}{s_s^2}, \qquad (5)$$

henceforth denoted as $\sigma_{\mathbf{v}}^2$.

For the calculations of sampling errors that follow, it is necessary to specify the spatial and temporal decorrelation scales, s_s and s_t. Stammer (1997) presented a global, latitudinally varying correlation function for SSH whose decorrelation scale is linearly related to the Rossby radius of deformation. While this function appears to provide a good description of the spatial correlation of SSH [Fig. 26b and Eqs. (13) and (19) in Stammer (1997)], it is not positive definite in either one or two dimensions (which may be demonstrated by direct numerical calculation of its Fourier and Hankel transforms) and thus cannot be used to calculate the sampling errors presented here. We therefore use the Gaussian forms given in Eqs. (2)–(4), with s_s chosen so that, for a given Rossby radius, C^{hh} has the same decorrelation scale as the function presented by Stammer (1997). The decorrelation scales used here are based on the global zonal average of the Rossby radii calculated by Chelton et al. (1998). To investigate the sensitivity of our results to the choice of s_s, we present sampling errors calculated using this ''nominal'' form and decorrelation scales larger and smaller by 25% at each latitude and henceforth referred to as the ''long'' and ''short'' decorrelation scales, respectively (Fig. 1a). The associated velocity standard deviations $\sigma_{\mathbf{v}}$, computed from (5) and normalized by the SSH standard deviation σ_h, are shown in Fig. 1b. For a given σ_h, the standard deviation of the velocity components decreases monotonically poleward. Note that the assumption that the decorrelation scale varies geographically violates the strict assumption of homogeneity. For the purposes of this analysis we thus assume that ''local'' homogeneity obtains, that is, that the SSH field is homogeneous over the region required for any specific velocity estimate. Temporal decorrelation scales s_t of 20 and 30 days will be considered (Stammer 1997).

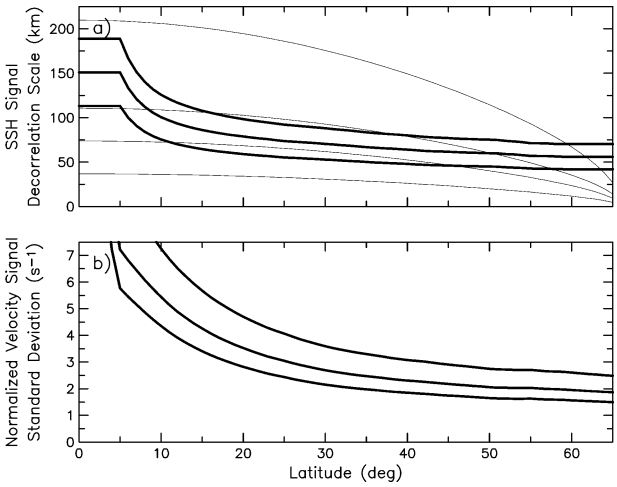

FIG. 1. (a) Variation with latitude of SSH decorrelation scales s_s for the nominal, short, and long cases (the middle, bottom, and top heavy solid lines, respectively). The thin lines are the track separation d in km for parallel tracks separated in longitude by $\delta\phi = 1.42°$, 0.75°, 0.5°, and 0.25° (top to bottom, see section 2b). (b) Variation with latitude of the velocity component signal std dev, normalized by the SSH signal std dev.

a. Velocity component estimation by the crossover method

1) CROSS-TRACK SPEED ESTIMATION

The basis for the crossover method is the estimation of cross-track speeds, which have also been used to calculate eddy kinetic energy with an assumption of isotropic velocity variability (e.g., Stammer 1997). The filtering properties and variance of cross-track speed estimates based on least squares line fits are described in this section.

Let β be the slope of SSH along a ground track at location x_j. At time t, the $M = 2M_{1/2} + 1$ measurements $\tilde{h}_{j+l}(t)$, $l = -M_{1/2}, \ldots, M_{1/2}$ are fit to a line by least squares. Dropping the dependence on t, and assuming that no data are missing, the estimate of the slope can be written as a linear combination of the data (Neter and Wasserman 1974),

$$\hat{\beta} = \sum_{l=-M_{1/2}}^{M_{1/2}} \alpha_l \tilde{h}_{j+l} = \sum_{l=-M_{1/2}}^{M_{1/2}} \alpha_l h_{j+l} + \sum_{l=-M_{1/2}}^{M_{1/2}} \alpha_l \epsilon_{j+l} + \sum_{l=-M_{1/2}}^{M_{1/2}} \alpha_l o_{j+l},$$

where

$$\alpha_l = \frac{x_{j+l} - \overline{x}}{\sum_{l=-M_{1/2}}^{M_{1/2}} (x_{j+l} - \overline{x})^2}$$

and $\overline{x} = M^{-1} \sum_{l=-M_{1/2}}^{M_{1/2}} x_{j+l} = x_j$ is the mean of the locations of the data along track. Note that the α_l do not vary with j. Since the measurements are evenly spaced

at intervals Δ_x along the ground track ($x_j = j\Delta_x$), some algebra leads to

$$\alpha_l = \frac{12l}{M(M^2 - 1)\Delta_x}.$$

Note that $\Sigma_{l=-M_{1/2}}^{M_{1/2}} \alpha_l = 0$. By assumption, the long-wavelength errors o_{j+l} are nearly constant for $l = -M_{1/2}, \ldots, M_{1/2}$, so that

$$\hat{\beta} = \sum_{l=-M_{1/2}}^{M_{1/2}} \alpha_l h_{j+l} + \sum_{l=-M_{1/2}}^{M_{1/2}} \alpha_l \epsilon_{j+l}. \quad (6)$$

The first term on the right-hand side of (6) is the expected value of $\hat{\beta}$ since $E[\epsilon] = 0$, where E denotes the expectation. Because SSH does not, in general, vary linearly along track, $E[\hat{\beta}]$ will differ from the true slope. The estimate (6) filters the true along-track SSH slope. The filtering characteristics of the least squares estimate of along-track SSH slope are directly related to the half-span $M_{1/2}$ over which the lines are fit. Since the least squares fit (6) is a linear operation, $E[\hat{\beta}]$ can be expressed in the wavenumber domain as

$$E[\hat{\beta}] = \int_{-\infty}^{\infty} \hat{P}^*(\zeta) H(\zeta)\, d\zeta, \quad (7)$$

where ζ is wavenumber, $H(\zeta)$ is the along-track power spectral density (PSD) of SSH, the asterisk denotes complex conjugation, and

$$\hat{P}(\zeta) = \sum_{l=-M_{1/2}}^{M_{1/2}} \alpha_l e^{-i2\pi\zeta x_{j+l}} \quad (8)$$

(Schlax and Chelton 1992). The transfer function $\hat{P}$ describes the filtering characteristics of the slope estimator in terms of how it filters the spectral components of SSH. By the derivative theorem (e.g., Bracewell 1986), the PSD of along-track SSH slope is related to the along-track PSD of SSH by $H'(\zeta) = i2\pi\zeta H(\zeta)$. The expectation (7) can therefore be expressed equivalently as

$$E[\hat{\beta}] = \int_{-\infty}^{\infty} \hat{P}'^*(\zeta) H'(\zeta)\, d\zeta, \quad (9)$$

where

$$\hat{P}'(\zeta) = \frac{\hat{P}(\zeta)}{i2\pi\zeta} \quad (10)$$

is the transfer function for the slope estimate in terms of along-track SSH slope (proportional to the cross-track component of geostrophic velocity).

Transfer function modulii $\|\hat{P}'(\zeta)\|^2$ are shown in Fig. 2a for three selected values of $M_{1/2}$. It is apparent that the slope estimate $\hat{\beta}$ is a low-pass-filtered version of the true slope. The wavelength λ_c of the half-power point of the low-pass filter increases linearly with increasing $M_{1/2}$ as shown in Fig. 2b. This filter cutoff is given approximately by

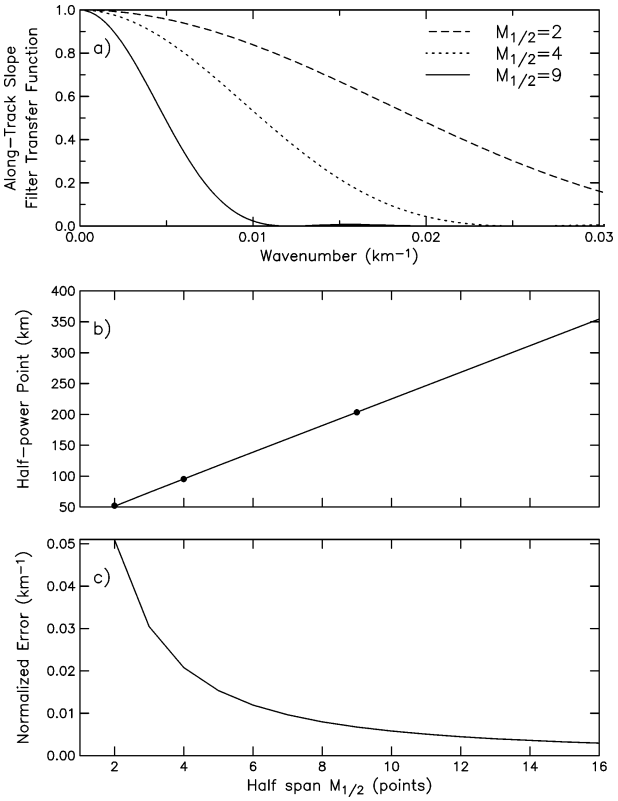

FIG. 2. (a) The filter transfer functions of the cross-track component of geostrophic velocity as estimated by local least squares fits of altimeter observations of SSH to a straight line over $2M_{1/2} + 1$ successive observations separated by 6.2 km. The transfer functions are shown for smoothing parameters of $M_{1/2} = 2$ (dashed line), $M_{1/2} = 4$ (dotted line), and $M_{1/2} = 9$ (solid line). (b) The solid line shows the linear relation between the half-power point of the filter transfer function and $M_{1/2}$. The dots show the half-power points for the specific filter transfer functions shown in (a). (c) The square root of the variance of the along-track slope estimate $\hat{\beta}$, normalized by the SSH error std dev σ_ϵ.

$$\lambda_c = 8.9 + 21.6\, M_{1/2}. \quad (11)$$

Mesoscale features with cross-track slopes that have length scales shorter than λ_c are attenuated by the least squares estimate of the SSH slope over $2M_{1/2} + 1$ successive observations. Increasing $M_{1/2}$ leads to slope estimates that more strongly filter the underlying SSH slope and thus are biased away from the true value of the slope at the estimation point. These smoother, more highly filtered estimates have inherently lower spatial resolution.

The second term on the right-hand side of (6) represents the effect of the measurement errors on $\hat{\beta}$; the variance of the along-track slope estimate can be shown to be

$$\mathrm{var}(\hat{\beta}) = \sigma_\epsilon^2 \sum_{l=-M_{1/2}}^{M_{1/2}} \alpha_l^2 = \frac{12\sigma_\epsilon^2}{M(M^2 - 1)\Delta_x^2}, \quad (12)$$

which is independent of the long-wavelength error variance. The dependence of $\sqrt{\mathrm{var}(\hat{\beta})}/\sigma_\epsilon$ on $M_{1/2}$ is shown

in Fig. 2c. Comparison of Figs. 2b and 2c shows the expected trade-off between the bias and the variance of the estimates: increasing $M_{1/2}$ leads to smoother estimates with lower variance.

The cross-track speed is estimated as $\hat{s}_\perp = g\hat{\beta}/f$, defined here to be positive to the left (right) of the along-track progression of the ground track in the Northern (Southern) Hemisphere. The error incurred when estimating cross-track speeds from along-track line fits may be quantified by the mean-squared error,

$$\Phi_{\hat{s}_\perp} = E[(s_\perp - \hat{s}_\perp)^2]$$

$$= \sigma_{\mathrm{v}}^2 - 2\frac{g}{f}\sum_{l=-M_{1/2}}^{M_{1/2}} \alpha_l E[s_\perp \tilde{h}_l] + \frac{g^2}{f^2}\sum_{k,l=-M_{1/2}}^{M_{1/2}} \alpha_k \alpha_l E[\tilde{h}_k \tilde{h}_l].$$

(Here and in the following, the dependence of the data $\tilde{h}$ on the along-track index j has been dropped.) For a ground track oriented at an azimuth γ measured clockwise from north, $s_\perp = -u\cos\gamma + v\sin\gamma$, whence

$$E[s_\perp h_l] = C_l^{s_\perp h} = -\cos\gamma C_l^{uh} + \sin\gamma C_l^{vh},$$

where C_l^{uh} and C_l^{vh} are, respectively, the covariances between h_l and the velocity components u and v at the location where $s_\perp$ is estimated. Defining C_{kl}^{hh} to be the covariance between h_k and h_l,

$$\Phi_{\hat{s}_\perp} = \sigma_{\mathrm{v}}^2 - 2\frac{g}{f}\sum_{l=-M_{1/2}}^{M_{1/2}} \alpha_l C_l^{s_\perp h} + \frac{g^2}{f^2}\sum_{k,l=-M_{1/2}}^{M_{1/2}} \alpha_k \alpha_l^u C_{kl}^{hh} + \frac{g^2}{f^2}\sigma_\epsilon^2 \sum_{l=-M_{1/2}}^{M_{1/2}} \alpha_l^2. \quad (13)$$

The first three terms on the right-hand side of (13) compose the expected squared bias of the estimate $E[(s_\perp - E[\hat{s}_\perp])^2]$. The fourth term is the variance of the estimate $E[(\hat{s}_\perp - E[\hat{s}_\perp])^2]$, cf. Eq. (12)}. The square roots of the expected squared bias and the variance will be referred to here as the sampling and measurement errors, respectively. The sampling error summarizes that part of the mse that results from the filtering imposed by the least squares fit, independent of the measurement error; it is the error that would be incurred with error-free measurements of SSH. The measurement error quantifies that part of the MSE that is due only to the errors in the SSH measurements. Equation (13) can also be expressed in the wavenumber domain in terms of SSH and the along-track slope PSD using Eqs. (7)–(10) and various properties of stationary random fields.

The sampling errors are shown in Fig. 3 as percentages of σ_{v} (appropriate to the particular decorrelation scales with $\sigma_h = 10$ cm) for three choices of filtering, $M_{1/2} = 2$, 4, and 9 (corresponding to cutoff wavelengths $\lambda_c = 50$, 100, and 200 km). Heavy solid, dashed, and dotted lines denote the sampling errors corresponding, respectively, to the nominal, long, and short variations of s_s with latitude. For $M_{1/2} = 9$, the maximum amount of filtering considered here (Fig. 3c), the sampling errors are the largest among the three levels of filtering and vary strongly with both latitude and the choice of decorrelation scale. At low latitudes, where the decorrelation scales are the longest (Fig. 1a), the sampling errors are minimum, indicating that there is only a small

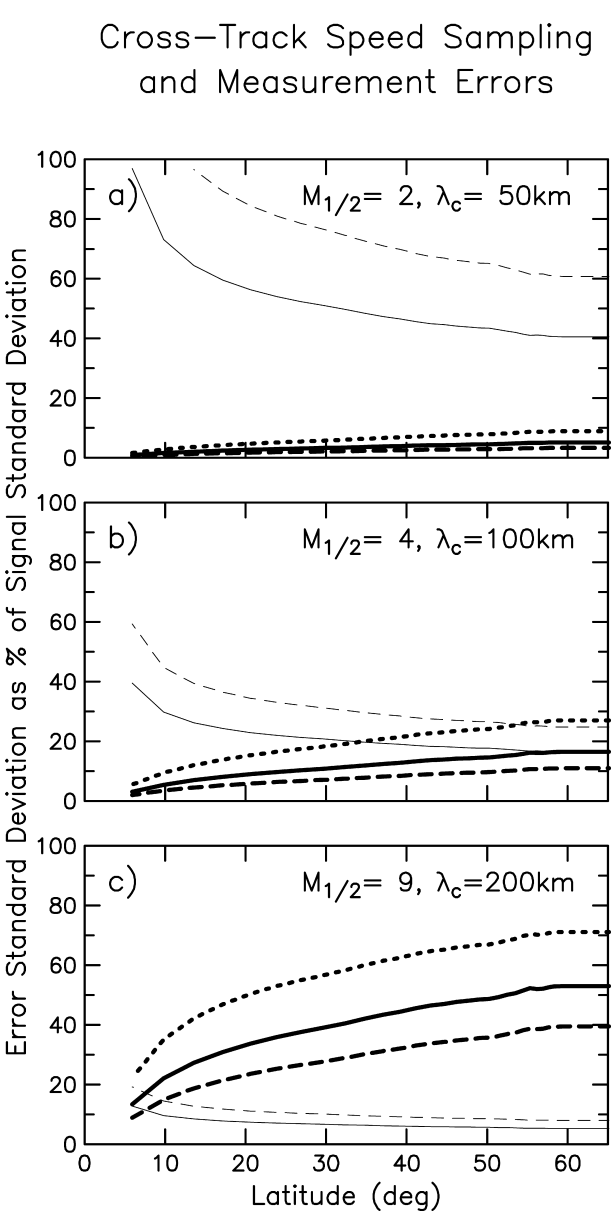

FIG. 3. Sampling and measurement errors for cross-track speeds estimated from along-track SSH data. In each panel the heavy solid, dashed, and dotted lines are the sampling errors calculated assuming the nominal, long, and short decorrelation scales, respectively, all normalized by the value of σ_{v} appropriate to $\sigma_h = 10$ cm and the assumed decorrelation scale. The thin solid and dashed lines in each panel are the cross-track speed estimation errors for SSH measurement errors with $\sigma_\epsilon = 2$ and 3 cm, respectively, normalized by σ_{v} assuming the nominal decorrelation scales. The calculations were done for three different along-track line fits: (a) $M_{1/2} = 2$, $\lambda_c \approx 50$ km, (b) $M_{1/2} = 4$, $\lambda_c \approx 100$ km, and (c) $M_{1/2} = 9$, $\lambda_c \approx 200$ km.

amount of short-scale energy to be attenuated in the velocity field. At higher latitudes, where the decorrelation scales decrease, the sampling error increases, indicating that the shorter scales present in the velocity field are attenuated by the along-track line fits. The sampling errors also increase as the overall decorrelation length scale decreases, so that the errors corresponding to the heavy dashed lines are always smaller than the errors corresponding to the heavy solid lines, which in turn are smaller than those corresponding to the heavy dotted lines. The other two cases with $M_{1/2} = 2$ (Fig. 3a) and $M_{1/2} = 4$ (Fig. 3b) show similar characteristics, but with lower overall relative sampling errors than the $M_{1/2} = 9$ case. For the $M_{1/2} = 2$ case, the sampling errors are less than 10% at all latitudes for all choices of spatial decorrelation scales because the minimum decorrelation scale of $s_s = 42$ km is not substantially shorter than the 50-km half-power point of the $M_{1/2} = 2$ filter.

The variations of the measurement errors with latitude and $M_{1/2}$ are opposite to those of the sampling errors. Measurement errors expressed as a percentage of σ_v [calculated using the nominal form for the latitudinal variation of s_s in Eq. (5) and an assumed SSH signal standard deviation of $\sigma_h = 10$ cm] are plotted in Fig. 3 for $\sigma_\epsilon = 2$ cm (thin solid lines) and $\sigma_\epsilon = 3$ cm (thin dashed lines). The measurement error of $\hat{s}_\perp$ increases toward the equator more rapidly than σ_v, resulting in a monotonic equatorward increase of the relative measurement error. The effect of increased smoothing is a dramatic reduction of the measurement error, a reflection of the fact that the variance of the slope estimates depends approximately on the inverse cube of $M_{1/2}$ [Eq. (12)].

Comparison of the measurement and sampling errors in Fig. 3 shows the previously noted trade-off between sampling and measurement error, that is, between the bias and variance of the speed estimates: increasing the along-track smoothing increases the bias while decreasing the variance. Of the three levels of filtering considered here, $M_{1/2} = 4$ comes the closest to balancing this trade-off. Less filtering ($M_{1/2} = 2$) results in very low bias with high variance, while more filtering ($M_{1/2} = 9$) sharply reduces the variance at the expense of incurring high levels of bias.

The bias–variance trade-off is summarized by the sum of the sampling and measurement errors, the mse (13). Figures 4a and 4b display the square root of the mse (the rmse) as a percentage of σ_v for $M_{1/2} = 2$, 4, and 9 (respectively, the dotted, solid, and dashed thin lines), for SSH measurement errors with $\sigma_\epsilon = 2$ and 3 cm. The nominal decorrelation scales are assumed, as is $\sigma_h = 10$ cm. Except at the lowest latitudes, $M_{1/2} = 4$ does provide the lowest overall error for these three choices of $M_{1/2}$. Poleward of about 25°, the relative rmse for $M_{1/2} = 4$ and $\sigma_\epsilon = 2$ cm is nearly constant at about 25%, while for $\sigma_\epsilon = 3$ cm it remains near 30% poleward of 30°. At lower latitudes, the effect of the f^{-2} dependence of the variance begins to dominate the total error except for the $M_{1/2} = 9$ case.

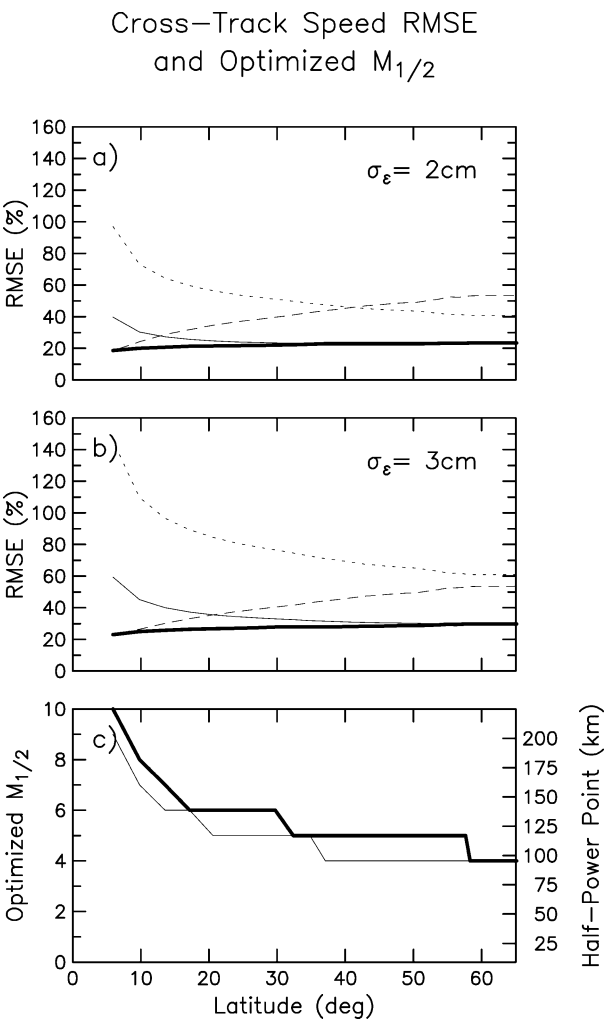

FIG. 4. Normalized rmse of cross-track speeds for $M_{1/2} = 2$ (dotted line), $M_{1/2} = 4$ (thin solid line), and $M_{1/2} = 9$ (dashed line) for (a) $\sigma_\epsilon = 2$ cm and (b), $\sigma_\epsilon = 3$ cm; and (c) the optimized value of $M_{1/2}$ for which the minimum rmse is obtained at each latitude for $\sigma_\epsilon = 2$ cm (thin line) and $\sigma_\epsilon = 3$ cm (heavy line). (c) The half-power points of the along-track slope filter transfer functions associated with the values of $M_{1/2}$ are labeled on the right axis. In (a) and (b) the heavy solid lines are the minimum rmse obtained with the latitudinally varying optimized value of $M_{1/2}$.

It is possible to find for each latitude the value of $M_{1/2}$ that minimizes the rmse. The minimum relative errors so calculated under the stated assumptions are shown as the heavy solid lines in Figs. 4a,b. The values of $M_{1/2}$ that minimize the total error (referred to here as the ''optimized'' $M_{1/2}$), and the corresponding SSH slope filter cutoff wavelength, are shown in Fig. 4c; discontinuities are the result of the integer values of $M_{1/2}$. The increase of the decorrelation length scales toward low latitudes allows the application of larger $M_{1/2}$ without increasing the sampling error. These larger spans also significantly decrease the variance of $\hat{s}_\perp$,

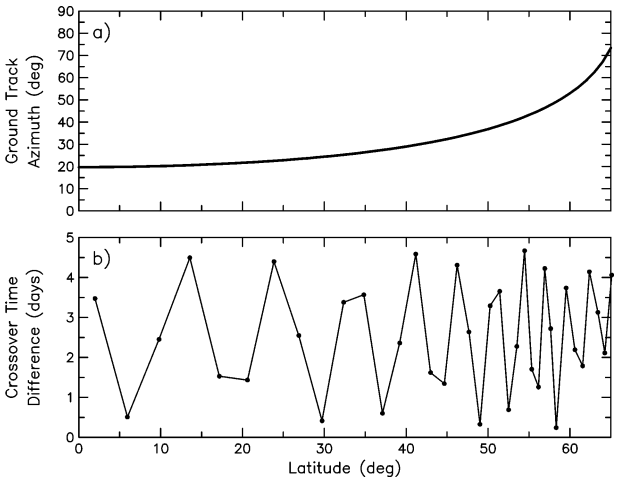

FIG. 5. Variation with latitude of (a) the ground-track azimuth γ, and (b) the time offset δ_t between SSH measurements on ascending tracks and descending tracks at crossovers.

with the result that the optimized $M_{1/2}$ increases from 4 at the highest latitudes to values near the equator of 9 for $\sigma_\epsilon = 2$ cm and 10 for $\sigma_\epsilon = 3$ cm. This latitudinally varying filtering is quite effective at mitigating the equatorward increase of the variance, resulting in an rmse that is nearly constant with latitude.

2) VELOCITY COMPONENT ESTIMATION

The crossover method uses cross-track speed estimates $\hat{s}_a(t)$ and $\hat{s}_d(t)$ calculated, respectively, from the ascending and descending tracks at a crossover to obtain time series of zonal and meridional velocity components from the geometric transformations

$$\hat{u}(t) = \frac{\hat{s}_d(t) - \hat{s}_a(t)}{2\cos\gamma} \tag{14a}$$

$$\hat{v}(t) = \frac{\hat{s}_d(t) + \hat{s}_a(t)}{2\sin\gamma}. \tag{14b}$$

In these equations, γ is the azimuth (clockwise from north) of the ground tracks at the crossover (Fig. 5a; see also Parke et al. 1987). As will be seen, a critical point occurs at approximately 56° latitude where $\gamma = 45°$ and the ground tracks are orthogonal. Poleward of that latitude, the angle between the ascending and descending ground tracks (i.e., twice the azimuth) is greater than 90° and equatorward of 56° it is less than 90°. Ascending and descending passes occur individually at times that are multiples of the repeat period Δ_t of the satellite (9.9156 days for T/P). At a given latitude where crossovers occur, temporally proximal ascending and descending passes are separated by a time interval $\delta_t \leq \Delta_t/2$ (Fig. 5b). The estimation times t in Eqs. (14) are centered at the midpoint between the nearest ascending and descending passes. Here $\hat{s}_a(t)$ and $\hat{s}_d(t)$ are the temporal linear interpolants of the cross-track speed estimates from the ascending and descending passes that occur just before and just after t.

Using Eqs. (6) and (14) and the formulas for linear interpolation, it is apparent that the velocity component estimates are each a linear combination of the $n = 4(2M_{1/2} + 1)$ data from the two ascending and two descending tracks about the estimation time t:

$$\hat{u}(t) = \sum_{i=1}^{n} \alpha_i^u \tilde{h}(x_i, y_i, t_i) \tag{15a}$$

$$\hat{v}(t) = \sum_{i=1}^{n} \alpha_i^v \tilde{h}(x_i, y_i, t_i), \tag{15b}$$

where (x_i, y_i, t_i) are the data locations in space and time.

The mse of the zonal component estimate at (x, y, t) is

$$\Phi_u(x, y, t) = \sigma_{\mathbf{v}}^2 - 2\sum_{i=1}^{n} \alpha_i^u C_i^{uh} + \sum_{i,j=1}^{n} \alpha_i^u \alpha_j^u C_{ij}^{hh} + \sum_{i,j=1}^{n} \alpha_i^u \alpha_j^u (\sigma_\epsilon^2 \delta_{ij} + \sigma_o^2 T_{ij}), \tag{16a}$$

where C_i^{uh} is the covariance between $u(x, y, t)$ and $h(x_i, y_i, t_i)$; C_{ij}^{hh} is the covariance between $h(x_i, y_i, t_i)$ and $h(x_j, y_j, t_j)$; δ_{ij} is the Kronecker delta; and $T_{ij} = 1$ if the data at (x_i, y_i, t_i) and (x_j, y_j, t_j) are on the same track, and 0 otherwise. Similarly,

$$\Phi_v(x, y, t) = \sigma_{\mathbf{v}}^2 - 2\sum_{i=1}^{n} \alpha_i^v C_i^{vh} + \sum_{i,j=1}^{n} \alpha_i^v \alpha_j^v C_{ij}^{hh} + \sum_{i,j=1}^{n} \alpha_i^v \alpha_j^v (\sigma_\epsilon^2 \delta_{ij} + \sigma_o^2 T_{ij}). \tag{16b}$$

As with the cross-track speed estimates, the first three terms on the right-hand sides of Eq. (16) compose the expected squared bias of the estimate. Since, by Eq. (12), var($\hat{\beta}$) depends approximately on $M_{1/2}^{-3}$, so will var($\hat{u}$) and var($\hat{v}$). [For the crossover estimates, the T_{ij} are redundant, since, as previously shown, the long-wavelength errors are filtered by the slope estimates. These terms are retained in Eq. (16) because of their pertinence for the parallel-track estimates in section 2b.]

The sampling errors for the short, nominal, and long decorrelation scales, and the three levels of filtering (i.e., $M_{1/2} = 2$, 4 and 9) are shown in Fig. 6, normalized in the same manner as the sampling errors in Fig. 3. Since estimation of the zonal and meridional velocity components involves temporal interpolation, the effects of differing temporal decorrelation scales are investigated by calculating the sampling errors for decorrelation timescale s_t of 20 and 30 days.

The sampling errors for the orthogonal velocity components are similar to those for the cross-track speed. Sampling errors vary directly with $M_{1/2}$ and inversely with the spatial decorrelation scale. For latitudes lower than 56°, sampling errors for $\hat{u}$ are smaller than those for $\hat{v}$ because the orientation of the ground tracks is

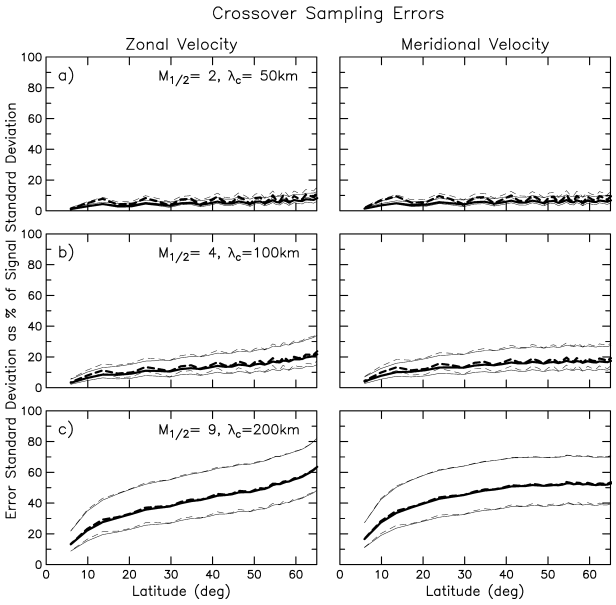

FIG. 6. Normalized sampling errors for crossover estimates of zonal and meridional velocity for the same values of $M_{1/2}$ as in Fig. 3. Solid and dashed lines show the errors assuming temporal decorrelation scales $s_t = 30$ and 20 days, respectively; heavy lines correspond to the nominal spatial decorrelation scales s_s; the upper and lower sets of thin lines correspond to the short and long decorrelation scales, respectively.

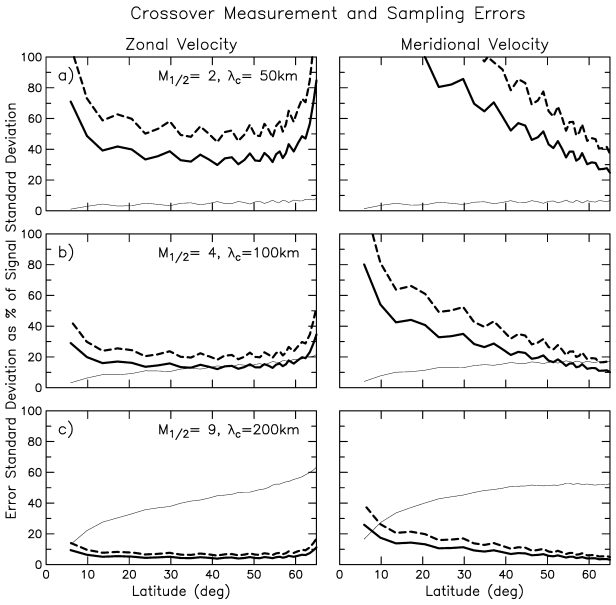

FIG. 7. Normalized measurement and sampling errors for crossover estimates of zonal and meridional velocity for the same values of $M_{1/2}$ as in Fig. 3. The heavy solid and dashed lines are the measurement errors for $\sigma_\epsilon = 2$ and 3 cm, respectively. The measurement errors are normalized by σ_v calculated assuming the nominal decorrelation scales and an SSH signal std dev of $\sigma_h = 10$ cm. The thin solid line is the normalized sampling error from Fig. 6 for the nominal decorrelation scales.

more favorable for estimating the zonal component when $\gamma < 45°$. The relative sampling errors for a temporal decorrelation scale of $s_t = 30$ days (solid lines) show a nearly smooth increase with latitude, while those for the 20-day decorrelation scale (dashed lines) have a more visible sawtooth pattern that reflects the sampling error associated with the temporal interpolation: the sampling errors are larger where the separation δ_t between the ascending and descending tracks is large (cf. Fig. 5b). This effect is most pronounced for $M_{1/2} = 2$ and 4; for $M_{1/2} = 9$ the effect of changing the temporal decorrelation is small compared to the large sampling error.

While $M_{1/2} = 2$ (Fig. 6a) yields very small sampling errors that, for the nominal spatial decorrelation length scales and $s_t = 30$ day case, do not exceed 10% of the signal, the relative measurement errors for $\hat{u}$ (Fig. 7a) exceed 30% and 50% for $\sigma_\epsilon = 2$ and 3 cm, respectively, at all latitudes. The relative measurement errors for $\hat{v}$ exceed 100% equatorward of 20° and 35° for the $\sigma_\epsilon = 2$ and 3 cm cases, respectively, and are never smaller than the 25% and 40% attained at the highest latitudes. Increasing $M_{1/2}$ to 4 reduces the measurement errors by more than a factor of 2, and increasing $M_{1/2}$ to 9 decreases the measurement errors by about another factor of 2. The measurement errors in both components increase toward the equator as a consequence of the f^{-1} dependence of the cross-track speed estimates. This effect is masked to a certain degree by the increase of the normalizing factor σ_v at low latitudes (see Fig. 1a).

The latitudinal dependencies of the measurement errors of $\hat{u}$ and $\hat{v}$ differ because of the factors cos γ and sin γ in the denominators of Eqs. (14). The measurement errors on $\hat{v}$ exceed those of $\hat{u}$ for latitudes lower than 56°, where sin $\gamma <$ cosγ. The reverse obtains at higher latitudes. The measurement errors for both components fluctuate in a sawtooth pattern that results from the temporal interpolation. The amplitude of this fluctuation is about 10% for $M_{1/2} = 2$, 5%–10% for $M_{1/2} = 4$, and a only a few percent for $M_{1/2} = 9$.

Comparison of Figs. 6 and 7 shows clearly the tradeoff between sampling and measurement error in the velocity component estimates. The single case of the sampling errors for the nominal spatial decorrelation and 30-day temporal decorrelation from Fig. 6 is overlaid as the thin solid line on Fig. 7. The total error for $M_{1/2} = 4$ and for estimates made with the latitudinally varying $M_{1/2}$ that minimizes the rmse of the cross-track speed estimates (Fig. 4c) are shown in Fig. 8 for $s_t = 30$ days and the nominal decorrelation scales. For $\sigma_\epsilon = 2$ cm, the rmse for $\hat{u}$ is near 20% between latitudes 10° and 50° and increases to 30% at 5° and 60° latitude. The rmse for $\hat{v}$ increases equatorward from a minimum of 20% at 65° latitude and exceeds 30% equatorward of about 35° latitude. The variable span filtering (Fig. 4c) is very effective for mitigating measurement error; for $\hat{v}$, the rmse of the filtered estimates remains near 30% to the lowest latitudes. The results for $\sigma_\epsilon = 3$ cm are similar, with somewhat larger rmse values.

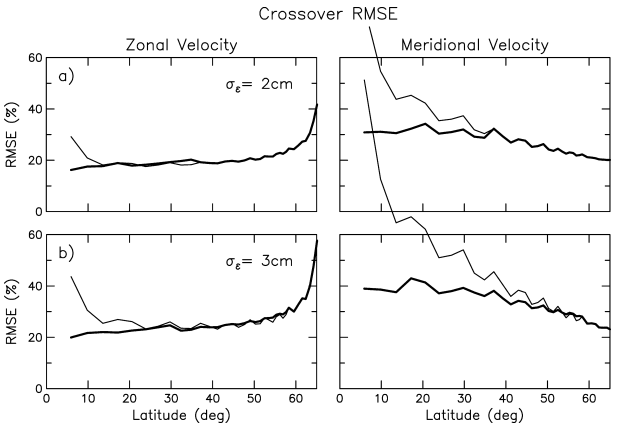

FIG. 8. Normalized rmse for crossover estimates of zonal and meridional velocity for (a) $\sigma_\epsilon = 2$ cm and (b) $\sigma_\epsilon = 3$ cm, assuming the nominal decorrelation scales. The thin lines and heavy lines show the rmse calculated for, respectively, a fixed value of $M_{1/2} = 4$ and for the latitudinally varying values of $M_{1/2}$ that minimize the rmse of cross-track speed estimates (Fig. 4c).

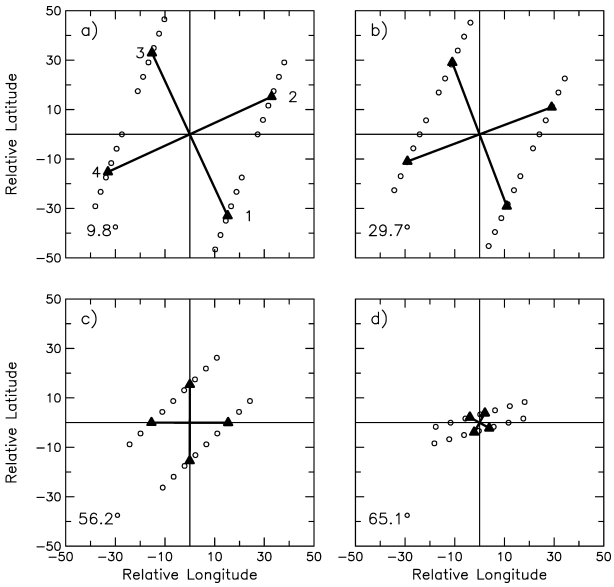

FIG. 9. Sampling geometry for the parallel-track method for $M_{1/2} = 2$ at latitudes of (a) 9.8°, (b) 29.7°, (c) 56.2°, and (d) 65.1°. Data locations are marked by the open circles. The locations of the four SSH estimates used to estimate orthogonal velocity components are shown by the solid triangles and labeled in (a). The pairs used to form the differences are connected by the heavy line segments that have length d, and the velocity estimates are at the intersections of the line segments. The axes are the latitude and longitude relative to the estimation location. The line segment 2–4 forms the angle $\omega = 45° - \gamma$ with the horizontal axis, where γ is the ground track azimuth (Fig. 5a).

b. *Velocity component estimation by the parallel-track method*

The parallel-track method developed by Stammer and Dieterich (1999) relies on differences of SSH between simultaneously measured parallel ground tracks to estimate the geostrophic velocity components (Fig. 9). The measurement locations denoted by the points 1–4 in Fig. 9a are selected so that the geostrophic velocity component estimates

$$\hat{u}' = \frac{g}{f}\frac{(\hat{h}_1 - \hat{h}_3)}{d} \tag{17a}$$

$$\hat{v}' = \frac{g}{f}\frac{(\hat{h}_2 - \hat{h}_4)}{d} \tag{17b}$$

are orthogonal. The four points are chosen so that the distances between the points 1 and 3 and between the points 2 and 4 are both d. These orthogonal velocity estimates can be rotated into the zonal and meridional components as

$$\hat{u} = \hat{u}'\cos\omega - \hat{v}'\sin\omega \tag{18a}$$

$$\hat{v} = \hat{u}'\sin\omega + \hat{v}'\cos\omega, \tag{18b}$$

where $\omega = 45° - \gamma$ and γ is the ground track azimuth (cf. Fig. 5a and section 2a). Note that at 56°, where $\gamma = 45°$, no rotation is required, and $\hat{u} = \hat{u}'$ and $\hat{v} = \hat{v}'$. For a track separation of $\delta\phi$ degrees of longitude, the distance between the points used to form the SSH differences at latitude θ is

$$d = 2\pi R_e \frac{\delta\phi}{360°}\frac{\cos\theta}{\cos 45°}\cos\gamma.$$

As originally proposed by Stammer and Dieterich (1999), the parallel-track method had no provision for along-track smoothing of the raw SSH data. In a subsequent analysis of the method, Leeuwenburgh and Stammer (2002) used along-track loess smoothing (Cleveland 1979) to reduce the effect of SSH measurement errors on the final velocity estimates. For analytical simplicity here, we use along-track averaging of the SSH data: each datum along the ground track is replaced by the average of itself and the nearest $M_{1/2}$ data points on each side along the track, yielding centered averages with $M = 2M_{1/2} + 1$ elements. Estimates of $\hat{u}'$ and $\hat{v}'$ [Eq. (17)] are then found by linearly interpolating the smoothed SSH to the required locations along track.

Given the availability of SSH data from a coordinated tandem altimeter mission, the parallel-track method has the advantage that the SSH measurements are simultaneous. This removes the need for the temporal interpolation required by the crossover method. The ground track geometry is rather more complicated, however. As the ground tracks converge poleward, the distance d over which the SSH differences (17) are formed decreases, imposing a latitudinally varying filtering of the underlying geostrophic velocity field. Leeuwenburgh and Stammer (2002) note that the poleward decrease of d will result in velocity estimates that can resolve shorter scales at higher latitudes, but do not quantify either the resolution or how it might be related to the latitudinal variation of the scales of SSH or velocity variability.

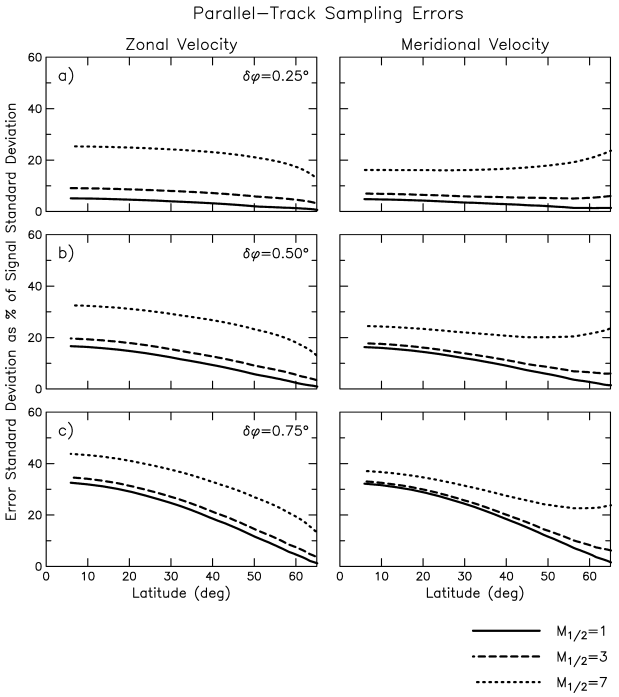

FIG. 10. Normalized sampling errors for parallel-track estimates of zonal and meridional velocity using a constant decorrelation scale s_s = 100 km for (a) $\delta\phi = 0.25°$, (b) $\delta\phi = 0.5°$, and (c) $\delta\phi = 0.75°$. The curves show the sampling errors for along-track averaging with $M_{1/2} = 1$ (solid), $M_{1/2} = 3$ (dashed), and $M_{1/2} = 7$ (dotted).

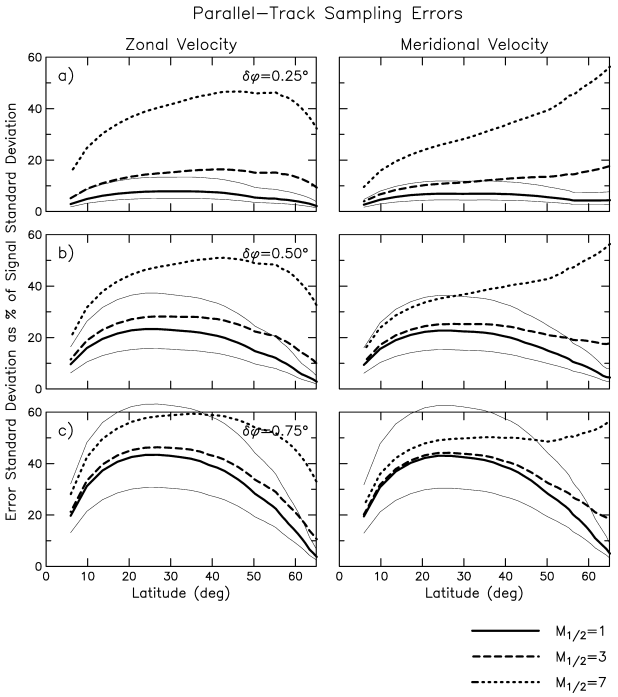

FIG. 11. The same as in Fig. 10, except using the nominal decorrelation scales with $M_{1/2} = 1$ (heavy solid), $M_{1/2} = 3$ (heavy dashed), and $M_{1/2} = 7$ (heavy dotted). The upper and lower thin solid lines are the normalized sampling errors for the short and long decorrelation scales, respectively, for the case of $M_{1/2} = 1$ only.

These issues are addressed here by calculating the sampling errors of the parallel-track estimates of velocity.

The parallel-track estimates of zonal and meridional velocity can be written in linear form, and the associated sampling errors can be calculated as was done for the crossover method in the previous sections [cf. Eqs. (15), (16)]. The latitudinal variation of the sampling errors is most easily understood by first considering a simplified example where a constant decorrelation scale $s_s = 100$ km is assumed; the case with the latitudinally varying decorrelation functions shown in Fig. 1 will be considered subsequently. Following Leeuwenburgh and Stammer (2002), sampling errors for three different ground track spacings ($\delta\phi = 0.25°$, 0.5°, and 0.75°) were calculated. The effects of three levels of along-track smoothing ($M_{1/2} = 1$, 3, and 7) were investigated. These values of $M_{1/2}$ result in along-track filtering of SSH with cutoff wavelengths of approximately 50, 100, and 200 km. The results are shown in Fig. 10.

Consider first the cases with $M_{1/2} = 1$. Equatorward of 56° latitude, the sampling errors for both components are identical, decreasing poleward along with d and increasing as the track separation $\delta\phi$ increases. These dependencies are expected: larger between-track spacing is less capable of resolving whatever short-scale variability is present in the geostrophic velocity field.

As $M_{1/2}$ is increased, the parallel-track velocity estimates resolve less short-scale variability, thus elevating sampling errors relative to those for $M_{1/2} = 1$. The effect of the increased smoothing is greater for $\hat{u}$ than for $\hat{v}$ for latitudes lower than 56°. Poleward of 56°, the smoothing with $M_{1/2} = 7$ also results in increasing sampling errors for $\hat{v}$. The reasons for this unexpected behavior and the difference between the sampling errors on u and v noted above are not readily apparent but must be related to the sampling geometry. The result is a filtering of the geostrophic velocity field that varies with latitude and is different for $\hat{u}$ than for $\hat{v}$.

Sampling errors for the nominal decorrelation scales (cf. section 2) show a more complicated behavior (Fig. 11). For $\hat{u}$, the sampling errors for all cases increase from the lowest latitudes, attain maximum values at midlatitudes, and then decrease toward the highest latitudes. Sampling errors for $\hat{v}$ exhibit similar behavior except for the cases with $M_{1/2} = 3$ and 7 for $\delta\phi = 0.25°$, and $M_{1/2} = 7$ for $\delta\phi = 0.5°$ and $\delta\phi = 0.75°$. Increasing $M_{1/2}$ from 3 to 7 dramatically increases the sampling errors. The nonintuitive, midlatitude maxima in the sampling errors can be understood with reference to Fig. 1a, in which the latitudinally varying values of d for the track separations $\delta\phi$ considered in Fig. 11 are overlaid as thin lines on the decorrelation scales assumed to obtain. For $\delta\phi = 0.75°$, it is clear that d exceeds the decorrelation scale between 10° and 50° and hence the estimates cannot resolve the short spatial scales at those latitudes. The relative magnitudes of d and s_s can apparently account for

much of the observed structure in the sampling error curves, but, as for the cases shown for the latitudinally constant decorrelation scale in Fig. 10, the precise origins of the high-latitude increase in the sampling errors for $\hat{v}$ and the differences between the sampling errors for $\hat{v}$ and $\hat{u}$ are not immediately apparent. Decorrelation scales shorter and longer than the nominal values cause substantial changes in the sampling errors when $M_{1/2} = 1$ and $\delta\phi$ is greater than 0.25°.

The poleward convergence of the ground tracks also affects the measurement errors. From Eqs. (18),

$$\mathrm{var}(\hat{u}) = \cos^2\omega\ \mathrm{var}(\hat{u}') - \sin 2\omega\ \mathrm{cov}(\hat{u}'\hat{v}') + \sin^2\omega\ \mathrm{var}(\hat{v}') \quad (19a)$$

$$\mathrm{var}(\hat{v}) = \sin^2\omega\ \mathrm{var}(\hat{u}') + \sin 2\omega\ \mathrm{cov}(\hat{u}'\hat{v}') + \cos^2\omega\ \mathrm{var}(\hat{v}'). \quad (19b)$$

From Eqs. (17),

$$\mathrm{var}(\hat{u}') = \frac{g^2}{f^2}\frac{\mathrm{var}(\hat{h}_1) + \mathrm{var}(\hat{h}_3)}{d^2} \quad (20a)$$

$$\mathrm{var}(\hat{v}') = \frac{g^2}{f^2}\frac{\mathrm{var}(\hat{h}_2) + \mathrm{var}(\hat{h}_4)}{d^2} \quad (20b)$$

$$\mathrm{cov}(\hat{u}'\hat{v}') = \frac{g^2}{f^2}\frac{\mathrm{cov}(\hat{h}_1\hat{h}_3) + \mathrm{cov}(\hat{h}_2\hat{h}_4)}{d^2}. \quad (20c)$$

Since $\mathrm{var}(\hat{u}') \approx \mathrm{var}(\hat{v}')$, it is apparent that $\mathrm{var}(\hat{u})$ and $\mathrm{var}(\hat{v}')$ differ by approximately $2\sin 2\omega\ \mathrm{cov}(\hat{u}'\hat{v}')$. Each of the four SSH estimates $\hat{h}_k$ appearing in Eqs. (17) is a linear combination of the SSH measurements (being the linear interpolant of two along-track averages) and can therefore be written as $\hat{h}_k = \sum \alpha_{kj}\tilde{h}_{kj}$ (where $\tilde{h}_{kj}$ is the jth data point used to in the estimation of $\hat{h}_k$), whence

$$\mathrm{var}(\hat{h}_k) = \sigma_\epsilon^2 \sum_j \alpha_{kj}^2 + \sigma_o^2 \sum_{i,j} \alpha_{ki}\alpha_{kj} \quad (21a)$$

$$\mathrm{cov}(\hat{h}_k\hat{h}_l) = \sigma_\epsilon^2 \sum_{i,j} \alpha_{ki}\alpha_{lj}\delta_{(ki),(lj)} + \sigma_o^2 \sum_{i,j} \alpha_{ki}\alpha_{lj}, \quad (21b)$$

where $\delta_{(ki),(lj)} = 1$ if the data locations correspond (i.e., if $\tilde{h}_{ki}$ and $\tilde{h}_{lj}$ are the same points), and 0 otherwise. Since all of the weights are positive for linear interpolation, so is $\mathrm{cov}(\hat{u}'\hat{v}')$.

The variances of $\hat{u}$ and $\hat{v}$ thus depend on d^{-2} and f^{-2} and increase poleward because of the former parameter and equatorward because of the latter. From Eqs. (19)–(21), it is apparent that the variances and, notably, their difference are also sensitive to the orbit error. An unexpected result following from Eq. (21b) is that, if the estimate pairs $\hat{h}_1$–$\hat{h}_3$ and $\hat{h}_2$–$\hat{h}_4$ are derived from any common points, the component variances will differ. This situation can occur depending on the latitude, track spacing $\delta\phi$, and the span $M_{1/2}$ over which the SSH estimates are constructed, but is mostly restricted to the highest latitudes (cf. Figs. 9c and 9d).

Figure 12 shows how the measurement errors for the parallel-track estimates of the velocity components depend on latitude, track spacing $\delta\phi$, and along-track smoothing $M_{1/2}$ for $\sigma_\epsilon = 2$ cm and orbit errors with $\sigma_o = 2$ cm. For comparison, to show the effects of the orbit errors, the case with $\sigma_o = 0$ cm is shown by the thin lines in Fig. 12. As in the previous figures in Section 2a, the errors are normalized by σ_v for $\sigma_h = 10$ cm and the nominal decorrelation scales. The curves show the expected increase of the errors at low and high latitudes and the general decrease at all latitudes as the track spacing $\delta\phi$ (and hence d) is increased. The measurement errors do not respond dramatically to changes of $M_{1/2}$, suggesting that care must be taken when smoothing to mitigate SSH measurement errors; the sampling errors from increased $M_{1/2}$ may increase more than the measurement errors decrease (cf. Fig. 11, Fig. 13, discussed below). For the case with no orbit errors, the differences between $\mathrm{var}(\hat{u})$ and $\mathrm{var}(\hat{v})$ exceed a few percent only for $\delta\phi = 0.25°$ or for latitudes higher than 56°. The effect of the 2-cm orbit error is marked, both in terms of the magnitude of the errors and the difference between the errors of the zonal and meridional component estimates at all latitudes. For $\delta\phi = 0.25°$, the errors for $\hat{v}$ with 2-cm orbit errors are off the scale of the plot.

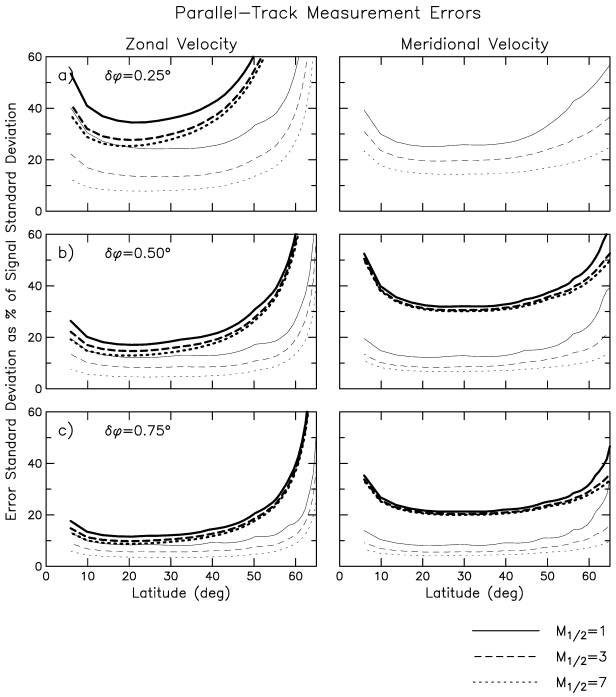

FIG. 12. Normalized measurement errors for parallel-track estimates of zonal and meridional velocity for the same values of $\delta\phi$ and $M_{1/2}$ as in Fig. 11, SSH measurement error $\sigma_\epsilon = 2$ cm, and orbit errors with $\sigma_o = 0$ and 2 cm (thin and heavy lines, respectively). (upper right) The heavy lines are off scale. The measurement errors are normalized as in Fig. 7.

The rmse of the parallel-track estimates shows how along-track smoothing can be detrimental (Fig. 13). For $\delta\phi = 0.5°$, for example, increasing $M_{1/2}$ from 3 to 7 nearly doubles the normalized rmse at midlatitudes for

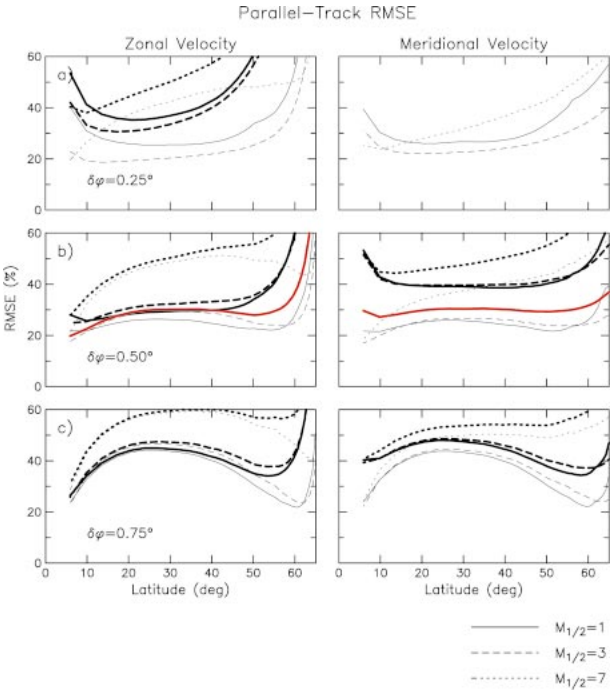

FIG. 13. Normalized rmse for parallel-track estimates of zonal and meridional velocity for the same values of $\delta\phi$ and $M_{1/2}$ as in Fig. 11, SSH measurement error $\sigma_\epsilon = 2$ cm, and orbit errors with $\sigma_o = 0$ and 2 cm (thin and heavy lines, respectively). (upper right) The heavy black lines are off scale; (middle) the red lines are the rmse's for $\delta\phi = 0.5$, $M_{1/2} = 1$ and $\sigma_o = 1$ cm.

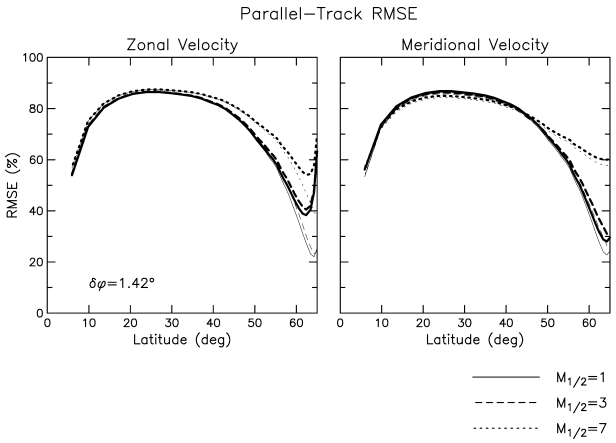

FIG. 14. The same as in Fig. 13, except for a ground track separation of $\delta\phi = 1.42°$ of the current tandem T/P–Jason mission. Note the change in the *y*-axis scale.

$\hat{u}$ and the minimum rmse occurs when $M_{1/2} = 1$. Thus, unlike the crossover method, increasing the along-track smoothing is not effective for reducing the rmse, a result of the relative insensitivity of the measurement errors to the along-track smoothing noted above.

The most favorable cases are those with $\delta\phi = 0.5°$ and $M_{1/2} = 1$ and 3. With these parameters and 2-cm orbit error, the rmse for $\hat{u}$ lies between 25% and 35% for latitudes between 5° and 50°. For the same latitude range, the rmse of $\hat{v}$ for these cases is between 40% and 45%. With no orbit error, the errors on $\hat{u}$ are decreased by a few percent over the latitude range 5°–40° and remain between 20% and 25% for latitudes up to 60°. The rmse of $\hat{v}$ for zero orbit error is between 20% and 25% for latitudes between 5° and 60°. Altimeters with residual orbit error less than 2 cm will have rmse's somewhere between these bounding values (e.g., the red line in Fig. 13, corresponding to $\sigma_o = 1$ cm).

As noted in the introduction, the current tandem T/P–Jason mission measures SSH simultaneously along parallel tracks with a longitudinal spacing of $\delta\phi = 1.42°$. The rmse of the parallel-track estimates from this mission are shown in Fig. 14. The 1.42° spacing leads to errors that are much greater than those resulting from the spacings considered in Fig. 13 because the wider track spacing is much less able to resolve the scales of variability present except at latitudes higher than about 59° (see the top thin line in Fig. 1a). The sampling error so dominates the rmse that the curves for both velocity components are similar, and neither orbit error nor smoothing has much effect on the results at most latitudes. The rmse for both $\hat{u}$ and $\hat{v}$ range between 55% and 85% for latitudes between 5° and 55°.

3. Summary and discussion

The results presented in the previous section provide a basis for comparing velocity estimates from the crossover and parallel-track methods. Some of the assumptions made, namely, the requirements that the velocity field be (at least locally) homogeneous and isotropic, are not quantitatively precise for some regions of the ocean. Nevertheless, the calculations allow a simple presentation of the general form of the errors of the methods and provide insight into the strengths and weaknesses of each.

The crossover method requires that cross-track speed estimates be interpolated to common times in order to transform them into zonal and meridional components. This interpolation introduces errors in the estimates. The calculations presented here based on SSH decorrelation timescales of 20 and 30 days suggest that this error is minimal for the 10-day repeat periods of the T/P and Jason orbits, resulting in rmse fluctuations of only a few percent. Both the zonal and meridional component measurement errors increase at low latitudes as a result of the f^{-1} dependence inherent in the geostrophic relation. The ground track geometry, embodied in Eqs. (14), enhances this effect for estimates of v and also results in elevated measurement errors for u at high latitudes. For latitudes lower than 56°, where the ground track azimuth γ is less than 45°, errors of $\hat{v}$ are larger than errors of $\hat{u}$. Poleward of 56° latitude, errors of $\hat{u}$ exceed those of $\hat{v}$. The magnitude of the difference depends directly on the standard deviation σ_e of the SSH measurement er-

rors. Ground track orientation also plays a role in the filtering of geostrophic velocity. Sampling errors based on the assumed decorrelation length scales increase systematically with increasing latitude for both velocity components.

The net effect of the changes in the sampling and measurement errors on crossover estimates of velocity is latitudinal variations of rmse that are quite different for the zonal and meridional components. At low latitudes, v cannot be estimated as reliably as u, while at high latitudes the situation is reversed. The sampling errors are also strongly dependent on the spatial decorrelation scale of the underlying SSH field. Along-track smoothing, implemented by increasing the span over which line fits are made, is quite effective at reducing the effects of measurement errors at low latitudes: measurement errors are reduced without incurring large increases in the sampling errors, resulting in lower rmse for both components. Even so, estimation errors are significant and exceed 20%–25% over most of the latitude range sampled by the T/P orbit.

The parallel-track method with simultaneous sampling of the two ground tracks obviates the need for temporal interpolation. On the other hand, the sampling geometry is more complex, which ramifies into both the measurement and sampling errors. As with the crossover method, the measurement errors increase at low latitudes as a consequence of the f^{-1} dependence of the estimates. The poleward decrease of the distance d over which the SSH differences are made also amplifies the measurement errors. As Eqs. (19)–(21) show, the sampling geometry results in a systematic difference between the measurement errors for $\hat{u}$ and $\hat{v}$ that changes with latitude and depends on the track separation $\delta\phi$, the degree of along-track smoothing $M_{1/2}$, and both the instrumental measurement and orbit errors. As for the crossover method, this difference is in the sense that errors of $\hat{v}$ are larger than errors of $\hat{u}$ equatorward of 56° latitude and errors of $\hat{u}$ exceed those of $\hat{v}$ poleward of that latitude. The sampling errors reflect the latitudinal variation of sampling geometry in a complex manner; the interplay between d and the decorrelation scale s_s causes sampling errors for both components to vary strongly with latitude with maxima at midlatitudes. Along-track smoothing is not very effective for mitigating measurement error and strongly affects the sampling error. For a track spacing of $\delta\phi = 0.5°$ with a 2-cm orbit error, the parallel-track method at midlatitudes is capable of producing estimates of u with errors of 20%–30% and of v with errors of about 40%. The errors of velocity estimates obtainable from the track spacing of $\delta\phi = 1.42°$ for the current T/P–Jason tandem mission are very large, between 55% and 85% for latitudes between 5° and 55° (Fig. 14).

Because of the difference in the sampling geometry of the two methods, direct comparison is difficult. The crossover method has a relatively simple relationship between the smoothing parameter $M_{1/2}$ and the filtering applied to the underlying velocity field. The parallel-track method does not allow such a straightforward characterization since the filtering is imposed by the ground track separation and varies latitudinally. It is therefore not clear which choice of smoothing parameters should be selected for each method when comparing their errors. An idealized comparison is available via the minimum errors obtained for the optimal estimates from each method. The optimal estimates are, by definition, those that minimize the mse for each method for the assumed signal and error statistics. The smoother weights for the two methods [α_i^u and α_i^v; cf. Eqs. (15)] that minimize the mean-squared errors are found in the usual manner by differentiating Eqs. (16) with respect to the smoother weights, setting the derivatives equal to zero, and solving the resulting linear system for the optimal weights. The estimates so found are optimal in the sense that the mse associated with these weights will be the minimum possible mse for any linear estimate, using the given data (e.g., the data appropriate to the crossover or parallel-track estimates) and the assumptions made about the statistics of the velocity field and errors.

Normalized optimal rmse's for the crossover method (heavy lines in Fig. 15) are almost invariant to changes in the assumed decorrelation scales, indicating that, for the correlation functions selected here, it is possible to choose sets of smoother weights that can adjust to the underlying spatial variability of the velocity field. For the crossover method, the normalized minimum rmse for $\hat{u}$ is nearly constant at 10% equatorward of about 50°. The errors for $\hat{v}$ show the expected variation with respect to those for $\hat{u}$, being about 20% near the equator and decreasing to 10% at 56°, poleward of which the errors of $\hat{u}$ exceed those of $\hat{v}$.

For the parallel-track configuration with the optimal track separation of $\delta\phi = 0.5°$, the errors of $\hat{u}$ are sensitive to the assumed decorrelation scales and to the orbit errors. For $\hat{v}$, the errors are less sensitive to the decorrelation scales but more sensitive to the magnitude of the orbit errors. There are systematic differences between the errors of $\hat{u}$ and $\hat{v}$.

The minimum parallel-track errors for $\delta\phi = 0.25°$ (not shown) are less sensitive to the choice of decorrelation scale, indicating that, for this case, the sampling geometry is able to adjust to the spatial variability of the velocity field. Errors for the shorter spacing increase more rapidly as the orbit error is increased. For $\delta\phi = 0.75°$ (also not shown), the results are more sensitive to the decorrelation scales because this wider track separation is less able to resolve short-scale variability.

Comparing the minimum errors for the crossover and parallel-track estimates with $\delta\phi = 0.5°$ in Fig. 15 shows that the former can provide better estimates of u at all latitudes. For orbit errors less than 1 cm, the parallel-track method yields errors in $\hat{v}$ that approximate the errors for the crossover method at low latitudes. For larger orbit errors, the errors of $\hat{v}$ from the parallel-track

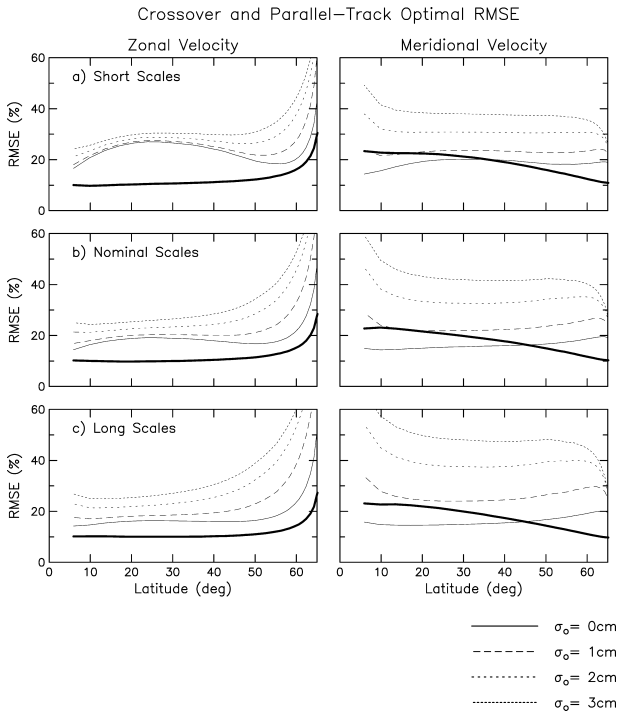

FIG. 15. Normalized rmse of optimal estimates for the crossover method (heavy solid line) and the parallel-track method with $\delta\phi = 0.5°$ (thin lines) for $\sigma_\epsilon = 2$ cm and a range of orbit error standard deviations σ_o for (a) short, (b) nominal, and (c) long decorrelation scales.

method are as large or larger than the errors from the crossover method at all latitudes.

It must be emphasized that these results hold only in the ideal case assumed here, wherein the true covariance function of SSH is known exactly, as are the variances and covariances of the SSH measurement errors. The minimum errors only serve to clarify the underlying properties of the estimates. In the reality of oceanographic data analysis, none of these statistical properties are actually known precisely. In particular, the spatial decorrelation scales of SSH vary geographically in a more complex manner than the simple latitudinal dependence assumed here (Fig. 1).

A more realistic, and correspondingly less simple, comparison of the two estimation schemes is provided by Leeuwenburgh and Stammer (2002), whose results rely on the approximation of reality provided by a high-resolution ocean circulation model. The errors they report are the differences between the ''truth'' of the model and simulations of the two estimation methods, averaged over large regions. Their results differ in some respects from those presented here. They suggest that the optimal track separation for parallel-track estimates is $\delta\phi = 0.75°$, compared to the 0.5° separation indicated by our results. The systematic differences between the errors on the parallel-track estimates of the zonal and meridional velocity components found here are not explicitly noted by Leeuwenburgh and Stammer (2002). They report that an advantage of the parallel-track method over the crossover method is that useful velocities can be obtained at all latitudes with comparable accuracy in the two components, an assertion that is contradicted by the results presented here; both methods have systematic differences in the errors of the two velocity components. With 2-cm orbit error and 2-cm SSH measurement error, they find total errors in parallel-track estimates of roughly 35% (with $\delta\phi = 0.75°$) on both velocity components in the Gulf Stream region. At the latitudes of the subtropical gyre and the Gulf Stream, they find errors of 20% and 40% in crossover estimates of the zonal and meridional components, respectively. While not identical, these error magnitudes are not substantially different from the results presented here.

4. Conclusions

Based on the assumption that surface currents are geostrophically related to an isotropic and locally stationary and homogeneous SSH field, sampling and measurement errors have been calculated for cross-track speed estimates and for estimates of the zonal and meridional velocity components using both the crossover and parallel-track methods. While the methods used to calculate the errors are general, they have been applied here specifically to the T/P and Jason orbits with 10-day repeat period and 66° orbit inclination.

It was shown that using along-track least squares line fits to SSH for the estimation of cross-track speeds allows a simple description of the filtering properties of the cross-track speed estimates. Since the crossover velocity estimates are derived from the cross-track speeds, they share the filtering properties of the cross-track speed estimates. Analysis of crossover estimates of velocity components shows how the component errors depend on latitude, SSH decorrelation scales, and measurement error. For the 10-day repeat period of the T/P and Jason orbits, the temporal interpolation required by the crossover method is not a major source of error for the 20- and 30-day decorrelation scales considered here. The geometry of the crossover sampling and the geostrophic relation lead to errors in crossover estimates that increase at low latitudes and are systematically different for $\hat{u}$ and $\hat{v}$. Errors in $\hat{u}$ are about 20% over the range 10°–50°. Poleward of 35°, errors on $\hat{v}$ decrease from about 30% to 20%. Equatorward of 35° the errors on $\hat{v}$ exceed 30%, although judicious along-track smoothing can extend this range and maintain the 30% error level on $\hat{v}$ to lower latitudes.

Sampling, measurement, and total errors show that the parallel-track method has similar limitations, but with different manifestations. Parallel-track estimates have sampling errors that vary in a rather complex manner with latitude and spatial decorrelation scale, the result of the varying filtering imposed by the poleward convergence of the ground tracks and other effects of the sampling geometry. Measurement errors on parallel-

track estimates are strongly dependent on orbit error, which also leads to systematic differences between the errors for the two component estimates. For a 2-cm residual orbit error and a track spacing of $\delta\phi = 0.5°$, $\hat{u}$ has total errors that range from 25% to 30% between 5° and 50°, while the errors on $\hat{v}$ are about 40% over the range 10°–50°.

If an arbitrary, but generous, threshold rmse of 30% of the velocity signal standard deviation for each orthogonal component is adopted, the crossover method has a range of useful application that extends from about 35° to 60° latitude with a fixed along-track smoothing parameter of $M_{1/2} = 4$ (Fig. 8a). Although restrictive, this includes the western boundary current extensions into the interior oceans in all basins and the energetic eddy regime of midlatitude eastern boundary currents. With the latitudinally varying optimized along-track smoothing shown in Fig. 4c, the reduction in the errors on $\hat{v}$ would extend this range equatorward to the lowest latitude of 5° considered here.

In comparison, the parallel-track method with the 30% threshold and a 2-cm orbit error and a track spacing of 0.5° cannot provide useful velocity estimates anywhere because errors in $\hat{v}$ exceed 40% at all latitudes (middle panels of Fig. 13). If the residual orbit error can be reduced to 1 cm, the rmse of $\hat{v}$ decreases to below the 30% threshold over the latitude range 5°–55° (see the red lines in Fig. 13 for $\delta\phi = 0.5°$, $M_{1/2} = 1$, and $\sigma_o = 1$ cm).

With the current track spacing of 1.42° in the current tandem T/P–Jason mission, the errors of the parallel-track method exceed 30% at all latitudes and exceed 80% at midlatitudes (Fig. 14). It seems unlikely that useful velocity estimates can be obtained from this dataset.

The results presented here show that both the crossover and parallel-track methods have limitations. Under optimistic assumptions on both, the methods appear to be roughly equivalent in terms of the range of useful estimates they can provide. While the crossover method may be able to achieve lower errors (at least in the idealized optimal case presented here), neither method stands out as being obviously inferior for the purpose of providing point estimates of geostrophic velocity. It is clear, however, that sampling (or filtering) properties are more easily understood for the crossover method than for the parallel-track method and that the effects of orbit errors on the latter method are substantial; successful application of the parallel-track method depends upon either orbit errors of 1–2 cm or their mitigation to that level at the data analysis phase.

Leeuwenburgh and Stammer (2002) suggest that one promising application of data from a tandem altimeter mission configured for parallel-track velocity estimation is the calculation of high-resolution along-track wavenumber spectra and covariances. The results here show that both the sampling and measurement errors for the parallel-track method change because of the poleward convergence of the ground tracks and other variations in the sampling geometry. If the interest in a dedicated parallel-track mission is the elucidation of along-track spectral characteristics of geostrophic velocity, the impact of these latitudinally varying effects on the interpretation of the spectra should be further investigated.

As noted, the methods used in this study are general and could be applied to analyze data from altimeter missions other than T/P and the tandem T/P–Jason mission considered here. The results for crossover estimates of velocity from SSH data obtained by European Remote Sensing Satellite (ERS) and *Envisat* can be anticipated based on the present analysis. ERS and *Envisat* are in exact-repeat orbits with a 35-day repeat period and 98° inclination. The 35-day repeat period will result in larger errors from the temporal interpolation than those reported here for 10-day orbit repeat period of T/P and Jason. The ground-track geometry imposed by the 98° orbit inclination will increase the errors on estimates of v relative to those from T/P or Jason crossover analyses.

Acknowledgments. We thank Olwijn Leeuwenburgh and Detlef Stammer for motivating the analyses presented in this study and for numerous discussions over the course of this study. We also thank Lee-Lueng Fu for very helpful comments on the original manuscript and for continued encouragement to carry out the statistical analyses of sampling and measurement errors in altimetric estimates of geostrophic velocity. We are especially grateful to Olwijn Leeuwenburgh for critical and constructive comments that lead to the inclusion of the effects of sampling errors that had been neglected in the original draft of the manuscript. The research presented in this paper was supported by Contract 1206715 from the Jet Propulsion Laboratory for funding of Jason Science Working Team activities.

REFERENCES

Bracewell, R. N., 1986: *The Fourier Transform and Its Applications.* McGraw-Hill, 474 pp.

Bretherton, F. P., R. E. Davis, and C. B. Fandry, 1976: A technique for objective analysis and design of oceanographic experiments applied to MODE-73. *Deep-Sea Res.*, **23,** 559–582.

Chelton, D. B., R. A. de Szoeke, M. G. Schlax, K. El Naggar, and N. Siwertz, 1998: Geographical variability of the first baroclinic Rossby radius of deformation. *J. Phys. Oceanogr.*, **28,** 433–460.

——, J. C. Ries, B. J. Haines, L.-L. Fu, and P. S. Callahan, 2001: Satellite altimetry. *Satellite Altimetry and the Earth Sciences: A Handbook for Techniques and Applications*, L.-L. Fu and A. Cazenave, Eds., Academic Press, 1–131.

Cleveland, W. S., 1979: Robust locally weighted regression and smoothing scatterplots. *J. Amer. Stat. Assoc.*, **74,** 829–836.

Ducet, N. P., and P. Y. Le Traon, 2001: A comparison of surface eddy kinetic energy and Reynolds stresses in the Gulf Stream and the Kuroshio Current systems from merged TOPEX/POSEIDON and *ERS-1/2* altimetric data. *J. Geophys. Res.*, **106,** 16 603–16 622.

——, ——, and G. Reverdin, 2000: Global high resolution mapping of ocean circulation from TOPEX/POSEIDON and *ERS-1/2. J. Geophys. Res.*, **105,** 19 477–19 498.

Leeuwenburgh, O., and D. Stammer, 2002: Uncertainties in altimetry-

based velocity estimates. *J. Geophys. Res.*, **107,** 3175, doi: 10.1029/2001JC000937.

Morrow, R., J. Church, R. Coleman, D. Chelton, and N. White, 1992: Eddy momentum flux and its contribution to the Southern Ocean momentum balance. *Nature*, **357,** 482–484.

——, R. Coleman, J. Church, and D. Chelton, 1994: Surface eddy momentum flux and velocity variances in the Southern Ocean from Geosat altimetry. *J. Phys. Oceanogr.,* **24,** 2050–2071.

Neter, J., and W. Wasserman, 1974: *Applied Linear Statistical Models.* Richard D. Irwin, Inc., 842 pp.

Parke, M. E., R. L. Stewart, D. L. Farless, and D. E. Cartwright, 1987: On the choice of orbits for an altimetric satellite to study ocean circulation and tides. *J. Geophys. Res.*, **92,** 11 693–11 707.

Qiu, B., 1995: Variability and energetics of the Kuroshio Extension and its recirculation gyre from the first two-year TOPEX data. *J. Phys. Oceanogr.,* **25,** 1827–1842.

Schlax, M. G., and D. B. Chelton, 1992: Frequency domain diagnostics for linear smoothers. *J. Amer. Stat. Assoc.,* **87,** 1070–1081.

Smith, R. D., M. E. Maltrud, F. O. Bryan, and M. W. Hecht, 2000: Numerical simulation of the North Atlantic Ocean at 1/10°. *J. Phys. Oceanogr.*, **30,** 1532–1561.

Stammer, D., 1997: Global characteristics of ocean variability estimated from regional TOPEX/Poseidon altimeter measurements. *J. Phys. Oceanogr.,* **27,** 1743–1769.

——, and C. Dieterich, 1999: Space-borne measurements of the time-dependent geostrophic ocean flow field. *J. Atmos. Oceanic Technol.,* **16,** 1198–1207.